Jestr

Journal of Engineering Science and Technology Review 17 (5) (2024) 191-198

Research Article

JOURNAL OF
Engineering Science and Technology Review

www.jestr.org

Numerical Simulation on Dynamic Recrystallization of the Thermal Deformation for 6061 Aluminum Alloy

Wei Zhang[1,*], Bo You[2] and Kun Ye[3]

[1]*RongCheng School, Harbin University of Science and Technology, Weihai 264300, China*
[2]*School of Automation, Harbin University of Science and Technology, Harbin 150080, China*
[3]*School of Material Science and Chemical Engineering, Harbin University of Science and Technology, Harbin 150080, China*

Received 8 August 2024; Accepted 20 October 2024

Abstract

6061 aluminum alloy is characterized by good comprehensive using properties and thermal processing performance. Traditional numerical simulation of 6061 aluminum alloy's thermal deformation is mostly limited to macroscopic deformation degree, stress-strain field, and deformation temperature field, which hinders accurately analyzing such microscopic phenomena as grain morphology change and dynamic recrystallization (DRX), thus affecting the precise quality control of the final parts. In order to simulate the dynamic recrystallization behavior during thermal deformation effectively, the hot compression experimental data were analyzed to establish the constitutive equation of flow stress and the critical equation of DRX. Then, the thermal deformation microstructure of 6061 aluminum alloy was numerically simulated based on Microstructure module of DEFRORM software , and the influencing laws of deformation amount, strain rate, and deformation temperature on the dynamic recrystallization were examined, followed by a comparative analysis with the deformation force, electron backscatter diffraction(EBSD)-based grain morphology, and transmission electron microscope (TEM)-based microstructure acquired in the hot compression experiment. Finally, the accuracy of the established models was verified. Results reveal that, as the deformation amount increased, the average grain size decreased; as the strain rate increased at a certain temperature, the size of the grains formed by dynamic recrystallization decreased, and the DRX volume fraction declined; as the temperature rose at a specific strain rate, the DRX volume fraction increased and the average grain size decreased. This study provides an important basis for optimizing the thermal deformation for 6061 aluminum alloy and regulating its structural performance.

Keywords: 6061 aluminum alloy, Dynamic recrystallization, Thermal deformation, Numerical simulation

1. Introduction

6061 aluminum alloy, as Al-Mg-Si series alloy, is one of the 6000 series aluminum alloys with low alloying and good properties. As a typical deformable heat-treated aluminum alloy, 6061 aluminum alloy possesses excellent corrosion resistance, welding performance, and processability. The common plastic processing methods for 6061 aluminum alloy are forging, extrusion, and rolling. 6061 aluminum alloy has strong corrosion resistance and mechanical properties after high-temperature plastic deformation, so it has been widely used in high-speed rail, automobiles, ships, building components, electronic equipment shells, and radiators [1-2]. Moreover, 6061 aluminum alloy has good comprehensive properties and thermal processing performance. The thermal deformation behaviors, such as dynamic recovery (DRV), dynamic recrystallization (DRX) and strain hardening, affect its microstructure and grain state, and then influence the final performance of the formed parts [3]. However, the research on the thermal deformation behavior mostly focuses on the qualitative analysis of the microstructure evolution after the hot compression experiment, and quantifying the high-temperature mechanical properties and microstructure evolution during thermal deformation by means of numerical simulation is rare. The DRX behavior during thermal deformation is complex and poses great challenges to the numerical simulation of its microstructure in thermal deformation.

Scholars have performed much work regarding the thermal deformation behavior and numerical simulation of deformation for 6061 aluminum alloy [4-5]. Nevertheless, the numerical simulation of 6061 aluminum alloy's thermal deformation mostly focuses on macro simulation, while its microstructure and dynamic recrystallization have been scarcely simulated. In addition, the built-in 6061 material libraries of simulation software and constitutive relations are inaccurate, and the stress and strain field is affected by the changes in different thermal deformation parameters during the thermal deformation and deviates from the actual technology. The microstructure evolution law of grains in the thermal deformation of 6061 aluminum alloy is also complicated. Hence, how to verify the constitutive relation of 6061 aluminum alloy effectively, accurately establish a numerical model with regard to its dynamic recrystallization, and deeply probe into the evolution law of its dynamic recrystallization is a problem to be urgently solved.

In this study, experimental characterization and numerical simulation were combined to establish the constitutive relation of flow stress and the critical equation of DRX. On this basis, the influencing laws of deformation amount, strain rate, and deformation temperature on DRX were explored. This study aims to predict the influence of thermal deformation on the microstructural evolution more accurately and further provide reference for developing and optimizing the precise forming of 6061 aluminum alloy.

*E-mail address: zhangw_hrbust@163.com
ISSN: 1791-2377
doi:10.25103/jestr.175.24

2. State of the art

Many Chinese and foreign scholars have extensively investigated the flow behavior and thermal processing map of 6000 series aluminum alloys. Wang et al. [6] studied the constitutive equation and thermal processing performance of 6061 aluminum alloy, and established the Arrhenius constitutive equation, but the microstructure evolution mechanism was seldom discussed. Jing et al. [7] established thermal processing map under different strains based on hot compression, analyzed and discussed the deformation behavior of AA6014 aluminum alloy, and obtained the best forming process window, but they did not explore the law of high-temperature flow stress. By performing the hot compression experiment of 6061 aluminum alloy, Chu et al. [8] constructed the constitutive equation of the thermal deformation of 6061 aluminum alloy and developed the DRX kinetic model, but the grain size model of dynamic recrystallization was not established, preventing predicting the change law of the dynamically recrystallized grain size. Hong et al. [9] performed axisymmetric isothermal compression experiments on 6063-T5 aluminum alloy, established the Arrhenius constitutive equation of adaptive coefficients and the dislocation density growth model, and obtained the best deformation temperature and deformation rate by drawing hot working maps, but less work was done on the change law of dynamic recrystallization. Ezatpour et al.[10] discussed the softening characteristics of 6061aluminum alloy during thermal deformation. The thermal simulation compression test showed that at 380 ℃ − 470 ℃ and 0.01 − 10 s^{-1}, the activation energy Q was obtained based on the Zener-Hollomon flow stress constitutive model as 274 kJ/mol. They concluded that the microstructure of the material is correlated with the Z parameter, and DRV and DRX occur only at a low value of Z parameter. Kopec et al. [11] discussed the mechanical properties and microstructure of 6061-T6 aluminum alloy at low temperature and performed hot compression experiments at −80 ℃. The strain rate under static conditions was 0.001 − 0.1 s^{-1}, and the strain rate under dynamic conditions was 1,250 − 3,400 s^{-1}. According to the electron backscatter diffraction (EBSD) analysis, the material deformation mechanism was dynamic recovery.

The dynamic recrystallization behavior of other series of aluminum alloys in case of thermal deformation has been extensively investigated, but the dynamic recrystallization and its microstructure evolution have been rarely studied via numerical simulation technology [12-14]. Chen et al. [15] proposed the model of thermal deformation-induced microstructure evolution and DRX for 7085 aluminum alloy, and systematically studied the effects of the temperature, deformation amount and strain rate on the thermal deformation microstructure evolution through isothermal compression tests. Zhang et al. [16] explored the DRX and microstructure evolution of Al-Mg-Si alloy during the thermal deformation. Based on the EBSD analysis, the DRX at 673 − 823 K and 0.01 − 10 s^{-1} was analyzed, the DRX kinetics equation and recrystallized grain size equation were constructed, and the elongated grain size and crystallized grain size during thermal deformation of the alloy were described, but the DRX mechanism was not investigated deeply. Liang et al. [17] studied the thermal deformation properties of A356 aluminum alloy, according to the DRX model of Arrhenius equation, the DRX volume fraction was accurately predicted by finite element analysis (FEA) software Forg, but the influence of strain rate on DRX was not analyzed. Xu et al. [18] analyzed the microstructure evolution of AA6063 aluminum alloy during thermal deformation, including DRV and DRX. At the temperature of 648 K, the microstructure evolution mechanism changed from DRV to DRX. The constitutive models of dislocation density, DRX volume fraction, and grain size were established, and the microstructure evolution of round bars during extruding deformation was numerically simulated, but the numerical simulation results of extruding deformation were not compared with experimental data. Gilmore et al. [19] studied the mechanical properties and microstructure evolution of AA2219 Al alloy during thermal torsional deformation. According to the high-temperature torsional moment curve and EBSD grain distribution, the DRX mechanism was analyzed, and the modified material constitutive model, DRX kinetics equation, and grain size equation were established. Based on ABAQUS software, the hot torsion of AA2219 Al alloy was numerically simulated. The results showed that the prediction accuracy of the recrystallization model was above 94%, and the prediction error of the grain size was within 11.5%, but the finite element modeling and boundary setting were not involved. Considering the DRX change during the profile extrusion of AA6082 aluminum alloy, Negozio et al. [20] presented a new method to evaluate the microstructure of fiber and DRX microstructure in 6061 aluminum alloy profiles based on Qform FEA software, and verified the extrusion experiment of AA6082 aluminum alloy round bars under several mold design and forming conditions. The results proved that the recrystallization in the extrusion of AA6082 aluminum alloy could be accurately predicted, but the influencing law of extrusion rate on dynamic recrystallization was not studied. Aiming at the high-temperature deformation properties and microstructure evolution of Ti-modified 2024 aluminum alloy, Gairola et al. [21] studied the deformation mechanism under different deformation conditions by empirical modeling, FEA and transmission electron microscope (TEM), and EBSD microstructure characterization, and concluded that the DRX mechanism was continuous DRX.

The above studies focused on the flow characteristic and thermal processing map of 6000 series aluminum alloy and the dynamic recrystallization behavior of other series of aluminum alloys during thermal deformation, without systematic discussion on the quantitative analysis of microstructure evolution during thermal deformation by numerical simulation technology and the influencing laws of forming process parameters on the dynamic recrystallization behavior. In this study, the constitutive equation of high-temperature flow stress and the critical equation of dynamic recrystallization were established by analyzing the hot compression experimental data. Next, the microstructure of 6061 aluminum alloy during thermal deformation was numerically simulated via the microstructure analysis module Microstructure of DEFRORM software, and the influencing laws of deformation amount, strain rate, and deformation temperature on the DRX of 6061 aluminum alloy were analyzed.

The remainder of this study is organized as follows. The constitutive relation, dynamic recrystallization model, and isothermal compression simulation finite element model of 6061 aluminum alloy are constructed in Section III. The correctness of the established constitutive relation is verified according to the forming force acquired during the hot compression experiment, and the influencing laws of deformation amount, strain rate, and deformation

temperature on the DRX volume fraction and DRX grain size. are explored in Section IV. The whole study is summarized, and the research conclusions are drawn in the final section.

3. Methodology

3.1 Constitutive relation and dynamic recrystallization model of 6061 aluminum alloy

(1).Constitutive relation of 6061 aluminum alloy

Because the flow stress is affected by factors such as the temperature, deformation amount, and strain rate when aluminum alloy materials are plastically deformed, the currently most widely applied Arrhenius constitutive relation equation, which was proposed by Sellars and Tegart, was adopted.

$$\dot{\varepsilon} = A\sinh(\alpha\sigma)^n \exp(-Q/RT) \tag{1}$$

where σ is the flow stress, MPa; Q stands for the activation energy, kJ/mol; R is the molar gas constant, 8.31 J/(mol·K); T is the absolute temperature, K; $\dot{\varepsilon}$ is the deformation rate, s^{-1}; A, n, α are material constants.

The finally solved constitutive relation equation of 6061 aluminum alloy is expressed as follows:

$$\dot{\varepsilon} = 2.6\times10^{17}\sinh(0.0151\sigma)^{8.93}\exp(-\frac{236.252}{8.314T}) \tag{2}$$

(2). Critical strain equation of dynamic recrystallization

According to the metallographic microstructural observation, the average grain size of the sample was 90 μm before deformation. ε_p (peak strain) and ε_c (critical strain) are defined in the microstructure module of finite element software DEFORM-3D as follows:

$$\varepsilon_p = a_1 d_0^{n_1}\dot{\varepsilon}^{m_1}\exp(Q_1/RT) \tag{3}$$

$$\varepsilon_c = \alpha\varepsilon_p \tag{4}$$

where d_0 is the original grain size; $\dot{\varepsilon}$ is the strain rate; Q_1 is the recrystallization activation energy; R is the gas constant; T is the thermodynamic temperature; n_1, m_1, and α are constants for the follow-up regression analysis.

Through the analytical calculation, the DRX critical strain equation is established as follows:

$$\varepsilon_p = 7.81\times10^{-4}\dot{\varepsilon}^{0.162}\exp(33872/RT) \tag{5}$$

$$\varepsilon_c = 0.8\varepsilon_p \tag{6}$$

(3). Kinetic equation of DRX

The DRX volume fraction model adopted in the microstructure analysis module of DEFORM software is the YADA model. For combining with this module, the following equations should be established:

$$X_{drex} = 1-\exp\{-\beta_d[(\varepsilon-a_{10}\varepsilon_p)/\varepsilon_{0.5}]^{k_d}\} \tag{7}$$

$$\varepsilon_{0.5} = a_5 d_0^{h_5}\dot{\varepsilon}^{m_5}\exp[Q_5/(RT)]+C_5 \tag{8}$$

where X_{drex} is the DRX volume fraction ; $\dot{\varepsilon}$ is the strain rate; $\varepsilon_{0.5}$ is the strain amount as dynamic recrystallization occurs by 50%; R and T are known constants; β_d, a_{10}, k_d, a_5, h_5, m_5, Q_5, and C_5 are the model parameters to be solved through regression.

Through the analytical calculation, the kinetic equation of dynamic recrystallization was established as follows:

$$X_{drex} = 1-\exp\{-1.0237[(\varepsilon-0.8\varepsilon_p)/\varepsilon_{0.5}]^{1.2624}\} \tag{9}$$

$$\varepsilon_{0.5} = 1.5\times10^{-4}\dot{\varepsilon}^{0.0232}\exp[42680/(RT)] \tag{10}$$

(4). DRX grain size equation

The DRX grain size model adopted in the microstructure analysis module of DEFORM software is as below:

$$d_{rex} = a_3 d_0^{h_3}\varepsilon^{n_3}\dot{\varepsilon}^{m_3}\exp[Q_3/RT] \tag{11}$$

where d_{rex} is the average grain size of DRX, d_0 is the original grain size; $\dot{\varepsilon}$ is the deformation rate, ε is the deformation amount, R is the gas constant, T represents the absolute temperature of deformation, and the other parameters are the equation coefficients to be calculated through regression.

Through the analytical calculation, the dynamically recrystallized grain size equation was established as shown below:

$$d_{rex} = 116.35\varepsilon^{0.615}\dot{\varepsilon}^{-0.115}\exp[-16280/RT] \tag{12}$$

3.2 Isothermal compression simulation finite element model for 6061 aluminum alloy

The hot compression samples were ϕ 8 mm×12 m cylinders. Because the compression samples were cylindrical and deformed in the form of axial symmetry, 1/12 parts of the compression samples were taken for the simulation. The upper and lower flat anvils were round and ϕ 60 mm×6 mm in size. Then, 3D modeling was designed in UG software, and the model was converted into STL format and imported into DEFORM-3D, as shown in Fig. 1.

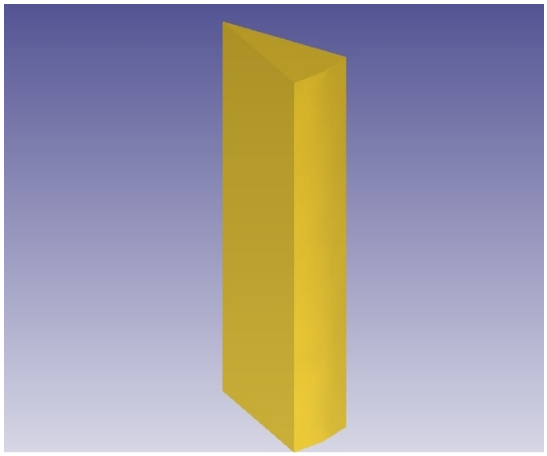

Fig. 1. Hot compression sample and geometric model

The constitutive relation and the dynamic recrystallization-related equations are shown in (2), (5), (6), (9), (10), and (12), which were imported into the microstructure analysis module Microstructure. Table 1 shows the numerical simulation process parameters for hot compression .

Table 1. Numerical simulation process parameters

Process parameter	Parameter value
Initial temperature/℃	350, 400, 450, 500
Mold temperature/℃	350, 400, 450, 500
Environmental temperature/℃	20
Friction coefficient	0.3
Heat transfer coefficient /N/mm/s/℃	180.181
Mold descent velocity/mm/s	0.12, 1.2, 12, 60
Initial grain size/μm	90

4. Result Analysis and Discussion

According to plastic forming theory, the cylindrical sample experienced nonuniform deformation in case of hot compression deformation. During the compression process, there are three deformation zones in the sample: the large , the free and the difficult deformation zone, as shown in Fig. 2. The large deformation zone was Zone I, namely, the outer edge of the sample's center and end. The free deformation zone was Zone III, namely, the outside of the sample's waist. The difficult deformation zone was Zone II, namely, the center of the sample end.

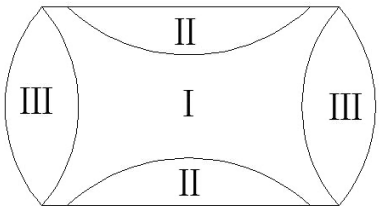

Fig. 2. Nonuniform deformation zones of hot compression sample

When the deformation temperature is 450 ℃ and the strain rate is 0.01 s^{-1}, the effective strain distribution at the deformation amount of 30%, 45%, and 60% are exhibited in Fig. 3. The effective strain distribution law of hot compression sample is consistent with the deformation situation described in Fig. 2.

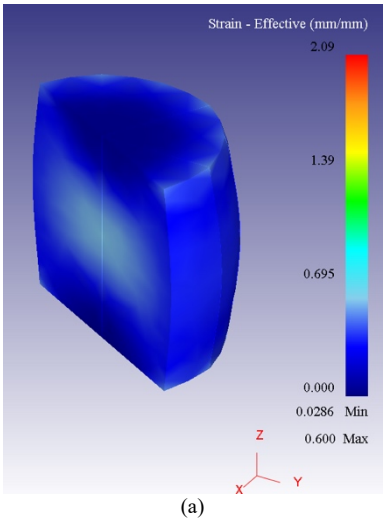

(a)

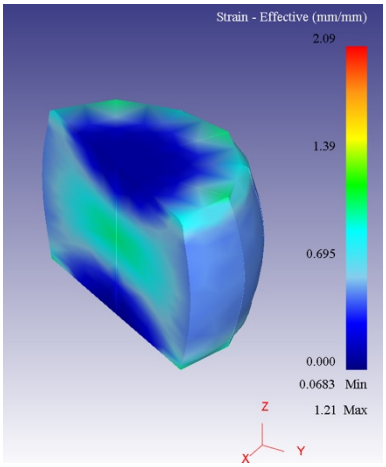

(b)

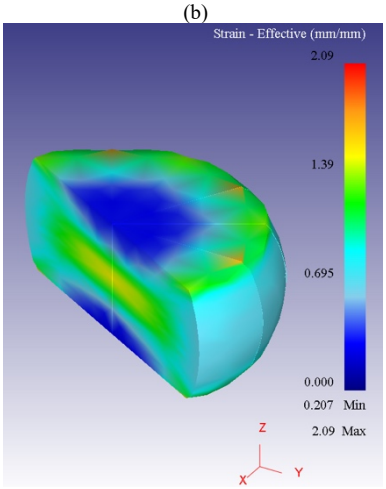

(c)

Fig. 3. Effective strain distribution under different deformation amounts. (a) 30%. (b) 45%. (c) 60%

4.1 Comparative analysis between simulated value and test value of forming force

When the deformation temperatures are 350 ℃, 400 ℃, 450 ℃, and 500 ℃ respectively, and the strain rates of 0.01 s^{-1} , 0.1 s^{-1} , 1 s^{-1} , and 5 s^{-1} , the hot compression experiment was simulated by the orthogonal experimental method, and the forming force-stroke curve was obtained. As shown in Fig. 4, which displays the forming force-stroke curve of the sample deformation at 0.01 s^{-1} and 350 ℃, 450 ℃. As shown in Fig. 5, the forming force-stroke curve of the sample deformation at 0.1 s^{-1} and 400 ℃, 500℃ are presented. Because the simulated finite element model was a 1/12 model, the obtained forming force was multiplied by 12 and the result was compared with the test value, as shown in Fig. 6.

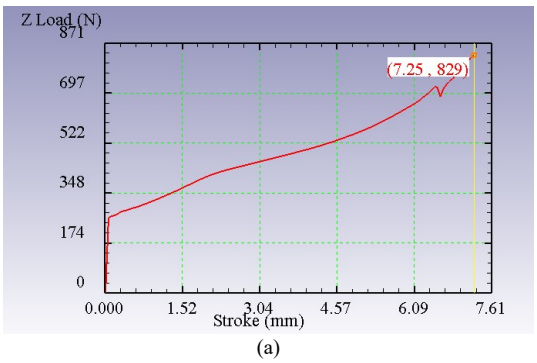

(a)

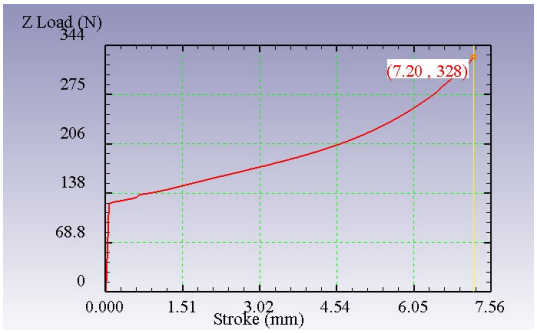

(b)

Fig. 4. Forming force - stroke curve at 0.01 s^{-1}. (a) 350 ℃. (b) 450 ℃.

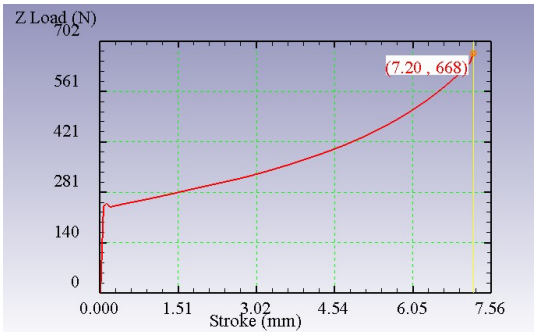

(a)

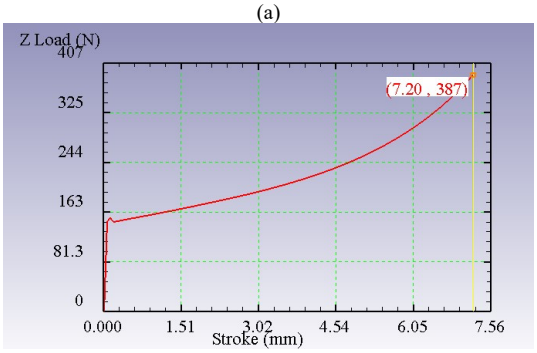

(b)

Fig. 5. Forming force - stroke curve at 0.1 s^{-1}. (a) 400 ℃. (b) 500 ℃.

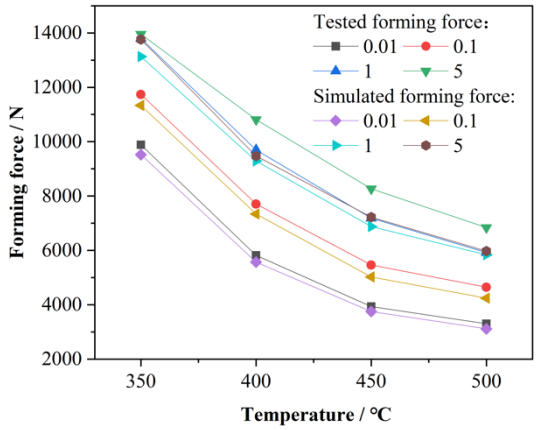

Fig. 6. Comparison between tested forming force and simulated forming force

Fig. 4-Fig. 6 reveal that overall, the tested forming force was smaller than the simulated forming force, the numerical error fell within 10%, and the established constitutive relation of 6061 aluminum alloy was highly accurate, which could reflect the relation between the flow stress and strain in case of thermal deformation well.

4.2 Influence of deformation amount on DRX

When the deformation temperature is 400 ℃, and the strain rate is 0.01 s^{-1}, the average grain size is shown in Fig. 7 at the deformation amounts of 20%, 40%, and 60%.

Fig. 7 shows that as the deformation degree increased, the average grain size gradually decreased. The DRX volume fraction was small under the deformation amount of 20%, which mainly occurred in the large and the free deformation zone. With the increase in the deformation amount, the areas without dynamic recrystallization in the difficult deformation zone gradually decreased. At the center of the sample's upper and lower end faces, the original grain size remained unchanged and was coarse. In the central zone of the sample, the grain refining effect was evident due to complete dynamic recrystallization. The free deformation zone at both sides of the sample was gradually transformed from partial DRX into complete DRX with the increase in the deformation degree. Upon the ending of deformation, except for the central zones of the upper and lower end faces, complete DRX took place in most zones, and the average grain size was about 17.0μm.

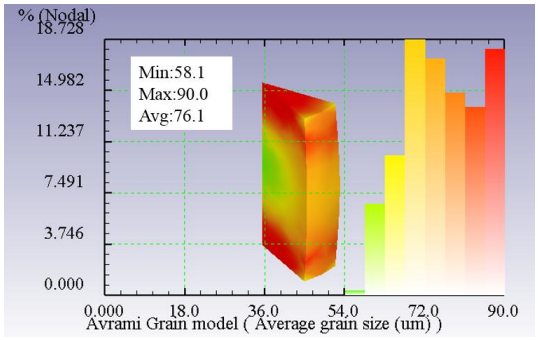

(a)

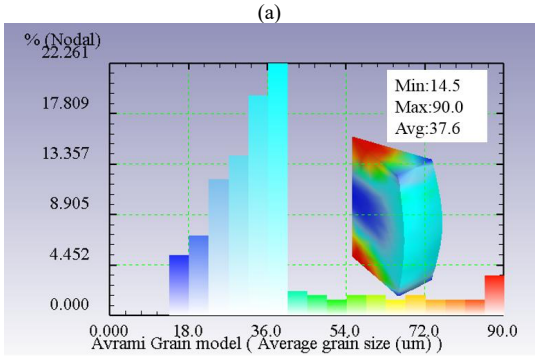

(b)

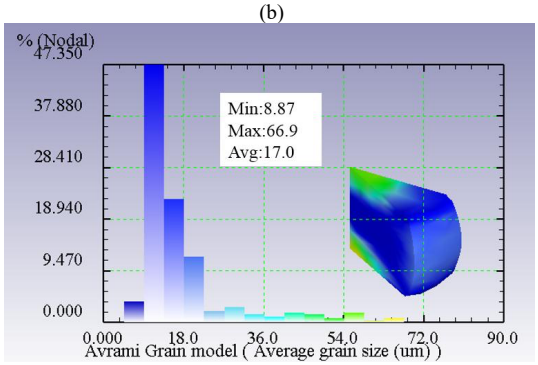

(c)

Fig. 7. Average grain sizes at different deformation amounts. (a) 20%. (b) 40%. (c) 60%

4.3 Influence of strain rate on DRX

Fig. 8 shows the changes in the DRX volume fraction at the deformation temperature of 400 ℃, deformation amount of 60%, and strain rates of 0.01 s^{-1}, 0.1 s^{-1}, and 1 s^{-1}.

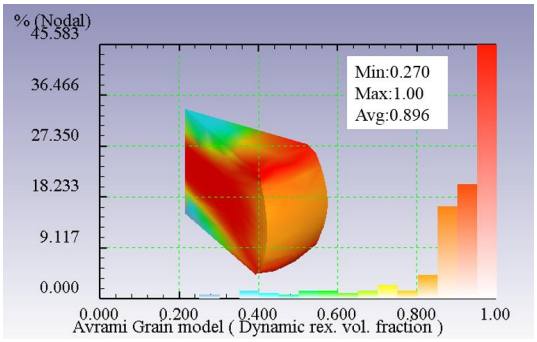

(a)

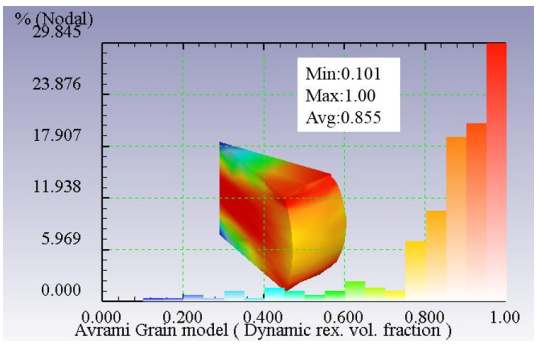

(b)

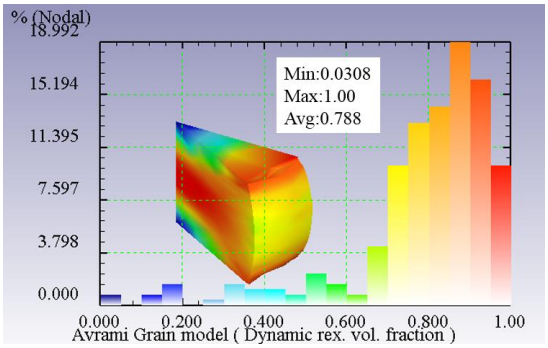

(c)

Fig. 8. DRX volume fraction at different strain rates. (a) 0.01 s^{-1}. (b) 0.1 s^{-1}. (c) 1 s^{-1} 1

Fig. 8 shows that as the strain rate grew, the DRX volume fraction gradually declined, which was mainly ascribed to the shortened deformation time and the increasing critical strain value . Many dislocations were generated and weakened the nucleation power at grain boundaries. The DRX volume fraction was 89.6% at 0.01 s^{-1}, 85.5% at 0.1 s^{-1}, and 78.8% at 1 s^{-1}. When the strain rate exceeded 1 s^{-1}, the overall DRX of the sample was not that ideal with few complete recrystallization zones. As the strain rate increased, the DRX grain size gradually decreased, but because the DRX volume fraction declined with the increasing strain rate, the number of dynamically recrystallized grains was reduced. Generally, the recrystallization fining effect was weakened, and the average grain size grew.

4.4 Influence of deformation temperature on DRX

Fig. 9 exhibits the average grain size distribution at the strain rate of 0.01 s^{-1}, deformation amount of 60%, and deformation temperatures of 400 ℃, 450 ℃, and 500 ℃. The average grain size was the largest in the difficult deformation zone of the sample's upper and lower end faces. When deformation ended at 400 ℃, the grain size at P3 was 56.1μm, the average grain size was small in the central large deformation zone because it was the first zone subjected to DRX, and partial DRX took place in the free deformation zone on the surface at both sides with 20.1μm. As the temperature grew, it gradually decreased, and the zone of DRX was continuously enlarged. When the temperature rose to 450 ℃, the grain size at P1 point approximated that at P2 point on the surface at both sides, the grain sizes at P1 and P2 were 8.1and 8.37μm, respectively. As the temperature grew to 500 ℃, except for the difficult deformation zone at the center of the upper and lower ends, the whole sample experienced dynamic recrystallization. Except for P3 point, the grain sizes at P1, P2, and P4 points were close to 7.3μm and indicated a substantial grain refining effect.

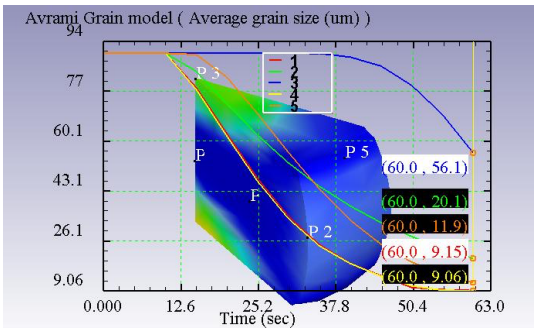

(a)

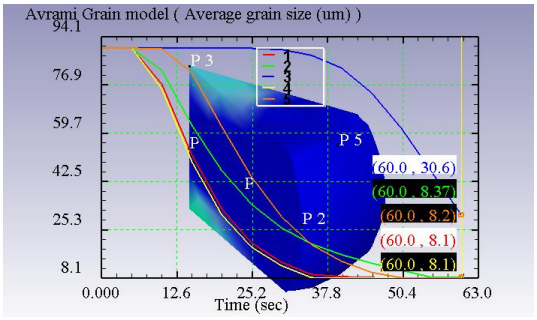

(b)

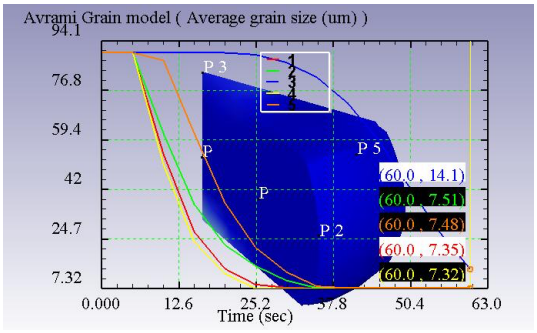

(c)

Fig. 9. Average grain sizes at different temperatures. (a) 400 ℃. (b) 450 ℃. (c) 500 ℃

4.5 Simulation result analysis of microstructure evolution

Fig. 10 displays the grain evolution at P1 point in the center of the large deformation zone at different strain moments during the hot compression deformation at 450 ℃ and 0.1 s^{-1}.

At the beginning of deformation, the grain size was coarse because it was the original grain structure. When the deformation amount grew to 20%, as shown in Fig. 10(b), nucleation started at the boundary of original grains. The main reason was that the dislocation density of 6061

aluminum alloy already reached the critical dislocation density and DRX started, but the grain size was very small at this moment. When the deformation amount reached 40%, grains were evidently enlarged, and DRX occurred in most zones with the original grains swallowed by new ones. At the deformation amount of 60%, complete DRX already took place, all grains stopped growing, and the grain sizes were distributed quite evenly.

The changes in the DRX grain size during the whole deformation are exhibited in Fig. 11. P1 point was the center of the Zone I, and P2 point was the location of the Zone III. When the deformation increases, the DRX grain size gradually grew. When the deformation ended, complete dynamic recrystallization occurred in the Zone I and Zone III, and the grain size was about 7.0μm, revealing an evident grain refining effect.

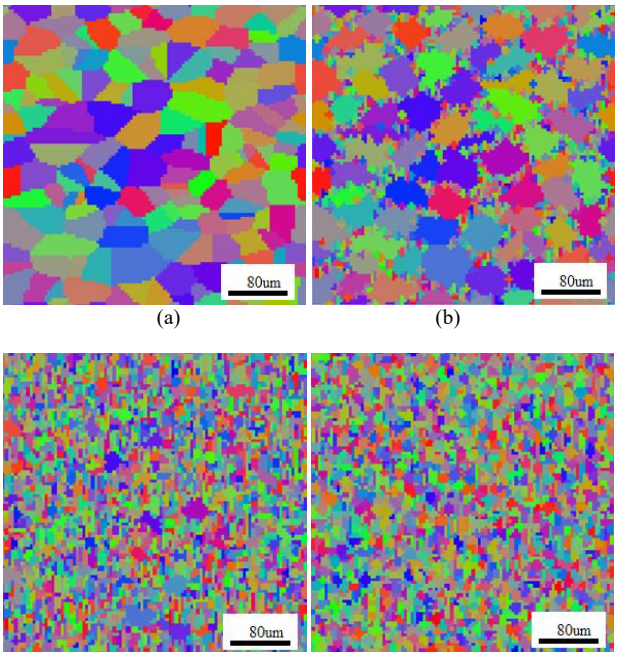

(a) (b)

(c) (d)

Fig. 10. Average grain sizes at different deformation amounts. (a) 0%. (b) 20%. (c) 40% (d) 60%

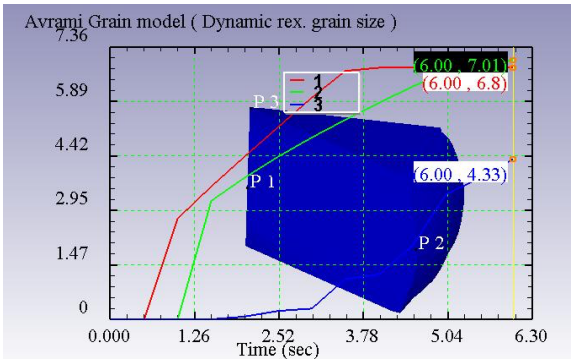

Fig. 11. Changes in DRX grain size

4.6 Comparison between simulation analysis and experimental results

Fig. 12 exhibits the EBSD analysis results and TEM microstructure at 450 ℃ and 0.01 s^{-1}. The recrystallization grains of the sample were refined markedly after the hot compression with clear boundaries. Moreover, the grain size coincided with the simulated value, indicating that the established DRX kinetic equation and grain size equation of 6061 aluminum alloy were accurate.

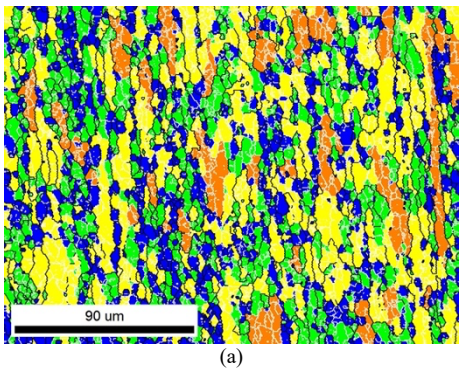

(a)

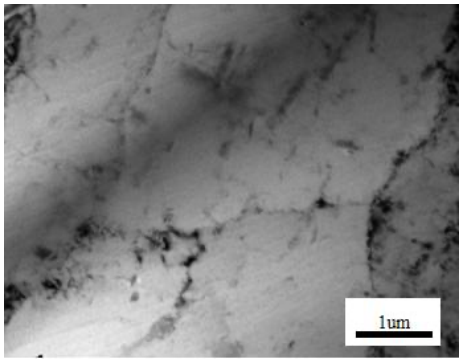

(b)

Fig. 12. Microstructures at 450 ℃ and 0.01 s^{-1}. (a) EBSD, (b) TEM

5. Conclusions

In this study, the numerical simulation of 6061 aluminum alloy's hot forming was organically combined with the quantitative description of its microstructure evolution to enhance the effectiveness and accuracy of its structural performance control. Aiming at such problems as the complex DRX behavior during the thermal deformation process, the flow stress constitutive equation and the DRX numerical model of 6061 aluminum alloy were constructed based on hot compression experimental data. Furthermore, the influencing laws of deformation amount, strain rate, and deformation temperature on the dynamic recrystallization and microstructure evolution were analyzed. Finally, the following conclusions could be drawn:

(1) Based on the simulation analysis of the forming force during the hot compression test, the forming force obtained through the analysis approximated the test value, and the numerical error was within 10%. This result verified that the established flow stress constitutive relation is accurate and reliable.

(2) The DRX behavior of 6061 aluminum alloy was explored. The average grain size decreased with increasing deformation. As the strain rate rose, the size of the grains formed by dynamic recrystallization decreased and the DRX volume fraction declined, while the final average size of the grain grew. As the temperature rose at a specific strain rate, the DRX volume fraction increased, and the average grain size decreased. The results demonstrate that the constructed DRX kinetic equation and grain size equation of 6061 aluminum alloy are accurate.

Experimental characterization and numerical simulation were combined to describe quantitatively the dynamic recrystallization behavior and grain morphology change laws during the thermal deformation of 6061 aluminum alloy, which are of great theoretical guiding significance. Because

the adopted experimental data were unavoidably affected by the material composition and heat treatment condition, corrections will be made in the follow-up study by combining variable optimization and numerical models to make the dynamic recrystallization model of 6061 aluminum alloy more accurate.

Acknowledgements

The study was supported by the Science and Technology Enterprise Innovation Ability Promotion Project of Shandong Province in China (Number 2022TSGC1307).

References

[1] P. F. Zhao, G. S. Ren, Z. Shen, and C. G. Xu, "Influence of hot compressive deformation conditions of 6061 aluminum alloy on flow stress and research on its constitutive equation," *J. Plast. Eng.*, vol. 14, no. 6, pp. 130-133, Dec. 2007.

[2] S. M. Mohseni, A. B. Phillion and D. M. Maijer, "Modelling the constitutive behaviour of aluminium alloy B206 in the as-cast and artificially aged states," *Mater. Sci. Eng. A*, vol. 649, pp. 382-389, Jan. 2016.

[3] G. H. Chen, L. Chen, G. Q. Zhao, C. S. Zhang, and W. C. Cui, "Microstructure analysis of an Al-Zn-Mg alloy during porthole die extrusion based on modeling of constitutive equation and dynamic Recrystallization," *J. Alloy. Compd.*, vol. 710, no. 7, pp. 80-91, Jul. 2017.

[4] H. X. Zhao, *et al*, "Abnormal grain growth behavior and mechanism of 6005A aluminum alloy extrusion profile," *J. Mater. Sci. Technol.*, vol. 157, pp. 42-59, Sep. 2023.

[5] R. Kalsar, *et al*, "Material flow behavior and microstructural refinement of AA6061 alloy during friction extrusion," *Mater. Charact.*, vol. 208, pp. 130-133, Feb. 2024.

[6] H. L. Wang, W. K. Liang, Q. T. Wang, and G. L. Lin, "Study on thermal deformation behavior and thermal processing map of aluminum alloy 6061," *J. Fujian Univ. Technol.*, vol. 20, no. 1, pp. 35-41, Feb. 2022.

[7] F. W. Jing, X. Y. Wu, X. G. Duan, P. Qiu, and H. T. Jiang, "Hot deformation behavior and hot processing map of AA6014 aluminum alloy," *J. Plast. Eng.*, vol. 28, no. 9, pp. 144-153, Sep. 2007.

[8] Z. J. Chu, B. Li, W. H. Wang, Y. Du, and Y. Sun, "Hot deformation behavior and dynamic recrystallization of 6061 aluminum alloy," *Rare Met. Mater. Eng.*, vol. 50, no. 7, pp. 2502-2510, Jul. 2021.

[9] H. Y. Hong, X. Y. Du and Z. G. Yan, "Study on hot deformation behavior and hot processing map of 6063-T5 aluminum alloy," *J. Light Ind.*, vol. 36, no. 4, pp. 86-96, Aug. 2021.

[10] H. R. Ezatpour, M. H. Sabzevar, S. A. Sajjadi, and Y. Huang, "Investigation of work softening mechanisms and texture in a hot deformed 6061 aluminum alloy at high temperature," *Mater. Sci. Eng. A-Struct. Mater. Prop. Microstruct. Process.,* vol. 606, pp. 240-247, Jun. 2014.

[11] M. Kopec, D. Gorniewicz, S. Jozwiak, J. Janiszewski, and Z. L. Kowalewski, "Microstructural evolution of 6061 aluminium alloy subjected to static and dynamic compression at low," *MRS Commun.*, vol. 13, no. 6, pp. 1244-1251, Dec. 2023.

[12] R. Kalsar, *et al*, "Material flow behavior and microstructural refinement of AA6061 alloy during friction extrusion," *Mater. Charact.*, vol. 208, pp. 1-11, Feb. 2024.

[13] V. P. Singh, G. K. Gupta, and S. Mishra, "Microstructural evolution and mechanical properties of multi-layered aluminum alloy 6061 processed by accumulative roll bonding," *J. Mater. Eng. Perform.*, pp. 1-12, Jun. 2024.

[14] X. D. Nguyen, Y. V. Gamin, T. K. Akopyan, and T. Y. Kin, "The deformation behavior and microstructure of aluminum alloy Al-6Mg-0.3Sc under conditions of hot forming," *Phys. Metals Metallogr.*, vol. 123, no. 11, pp. 1176-1184, Nov. 2022.

[15] X. H. Chen, K. H. Chen, P. X. Dong, G. S. Peng, and S. Y. Chen, "Microstructure evolution and dynamic recrystallization model of 7085 aluminum alloy during hot deformation," *Chin. J. of Nonferrous Met.*, vol. 23, no. 1, pp. 44-50, Jan. 2013.

[16] C. S. Zhang, *et al*, "Investigation of dynamic recrystallization and modeling of microstructure evolution of an Al-Mg-Si aluminum alloy during high-temperature deformation," *J. Alloy. Compd.*, vol. 773, pp. 59-70, Jan. 2019.

[17] Z. L. Liang, W. T. Li, B. G. Zhu, and L. Q. Niu, "Modelling dynamic recrystallization of A356 aluminum alloy during hot deformation," *Metals*, vol. 12, no. 9, pp. 1-8, Sep. 2022.

[18] L. Xu, *et al*, "Microstructure evolution, constitutive modeling and forming simulation of AA6063 aluminum alloy in hot deforming," *Mater. Today Commun.*, vol. 34, pp. 1-12, Mar. 2023.

[19] A. Gilmore and X. Liu, "Mechanical Behavior and Microstructure evolution during hot torsion deformation of aluminum alloy AA2219," *Adv. Eng. Mater.*, vol. 24, no. 9, pp. 1-15, Sep. 2022.

[20] M. Negozio, R. Pelaccia, L. Donati, and B. Reggiani, "Numerical investigation of the surface recrystallization during the extrusion of a AA6082 aluminum alloy under different process conditions," *Int. J. Adv. Manuf. Technol.*, vol. 129, pp. 1585-1599, Oct. 2023.

[21] S. Gairola, G. Singh, R. Jayaganthan, and G. Ajay, "High temperature performance of additively manufactured Al 2024 alloy: constitutive modelling, dynamic recrystallization evolution and kinetics," *J. Mater. Res. Technol-JMRT*, vol. 25, pp. 3425-3443, Jun. 2023.